Chapter 1

Scattering of Nucleons

"Although the study of the deuteron gives us a number of clues about the nucleon–nucleon interaction, the total amount of information available is limited... To study the nucleon–nucleon interaction in different configurations, we can perform nucleon–nucleon scattering experiments."

K. S. Krane

The deuteron (Lectures 7–9) is the only bound two-nucleon system. It samples the residual NN force in a single channel, mostly ${}^3S_1$ with a few-percent D-wave, at a fixed average separation fixed by weak binding. That is not enough to reconstruct the full force. There are no bound excited states to explore other partial waves or spin orientations, and the continuum is invisible from multipole moments alone [6].

Scattering supplies what the bound state cannot: controllable energy, access to $\ell = 0, 1, 2, \ldots$, and both spin channels. In this lecture the experimental definition of the cross section is tied to partial-wave analysis. Phase shifts δ_ℓ become the language in which theory and experiment meet for a short-range central potential [6, 1, 2, 14].

1.1 Why scatter neutrons on protons?

A scattering experiment uses a monoenergetic **projectile** beam and a **target** with many scattering centres. For n–p scattering the projectiles are neutrons of chosen kinetic energy and the target is hydrogen: each scattering centre is a free proton (bound only in the atom, irrelevant at nuclear energies). A detector at polar angle θ relative to the beam axis counts scattered particles. For a central force the yield does not depend on the azimuthal angle ϕ.

Hydrogen is essential for a clean NN measurement. On a heavy nucleus an incident nucleon would scatter from several target nucleons within the force range, so the observed yield would mix many-body effects. On hydrogen each encounter is a single np collision; multiple scattering from different atoms is rare if the target is thin [6]. The same philosophy motivates electron scattering on thin foils when one wants the elementary charge form factor (Lecture 1): isolate one interaction per projectile.

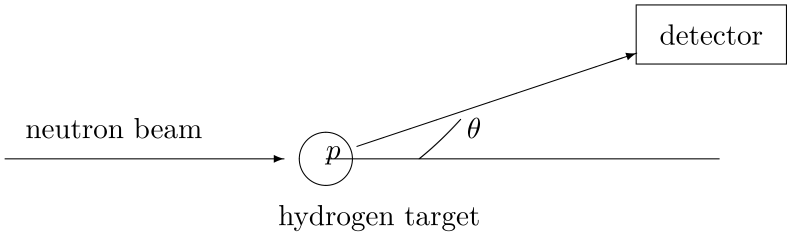

centre-of-mass angle; thin target isolates one np collision

Figure 1.1: Schematic n–p scattering setup: monoenergetic projectile beam, hydrogen target, and detector at angle θ.

1.2 Differential and total cross sections

The number $\mathrm{d}N$ of particles recorded in time t into solid angle $\mathrm{d}\Omega$ grows with exposure time, detector acceptance, beam intensity I (particles per unit area per unit time), and the number of target centres N_t (or areal density n_a times the illuminated area). These experimental knobs are factored out by defining the **differential scattering cross section** $\mathrm{d}\sigma/\mathrm{d}\Omega$ through

$$\mathrm{d}N = \frac{\mathrm{d}\sigma}{\mathrm{d}\Omega}\, t\,\mathrm{d}\Omega\, I\, N_t. \tag{1.1}$$

Equivalently,

$$\frac{\mathrm{d}\sigma}{\mathrm{d}\Omega} = \frac{\mathrm{d}N}{\mathrm{d}\Omega\, n_a\, N_p}, \qquad N_p = tIA, \tag{1.2}$$

with A the beam area. The cross section has dimensions of area; the historical unit is the barn,

$$1\,\mathrm{b} = 10^{-28}\,\mathrm{m}^2 = 100\,\mathrm{fm}^2.$$

Nuclear NN cross sections at low energy are tens of barns, huge compared with the geometric size of a nucleon ($\sim 1\,\mathrm{fm}^2$), a quantum enhancement characteristic of low-energy s-wave scattering [6, 1].

Physically, $\mathrm{d}\sigma/\mathrm{d}\Omega$ is the effective area that the target presents for scattering into $\mathrm{d}\Omega$. It packages all of the unknown dynamics into a measurable quantity: once $\mathrm{d}\sigma/\mathrm{d}\Omega$ is known, one can compare theories without redoing the experiment for every proposed potential.

Angles and energies may be quoted in the laboratory or centre-of-mass (CM) frame. Partial-wave formulae below are written in the CM frame; converting to laboratory angles for equal-mass np scattering is a standard kinematic exercise. The **total** elastic cross section is the angular integral

$$\sigma_{\mathrm{tot}} = \int \frac{\mathrm{d}\sigma}{\mathrm{d}\Omega}\,\mathrm{d}\Omega. \tag{1.3}$$

For pure s-wave scattering, $\mathrm{d}\sigma/\mathrm{d}\Omega$ is isotropic in the CM frame and $\sigma_{\mathrm{tot}} = 4\pi\,(\mathrm{d}\sigma/\mathrm{d}\Omega)$.

1.3 Central potential, plane waves, and partial waves

A **central** potential $V(r)$ depends only on the nucleon–nucleon separation. Angular momentum about the force centre is then conserved, so eigenstates of definite orbital angular momentum ℓ

are useful. In the absence of interaction the incident beam is a plane wave along z,

$$\psi_{\text{inc}} = e^{ikz}, \qquad k = \frac{p}{\hbar} = \frac{\sqrt{2\mu E}}{\hbar}, \tag{1.4}$$

where $\mu \approx m_N/2$ is the reduced mass of the NN system and E is the centre-of-mass kinetic energy. Multiplying by $e^{-iEt/\hbar}$ makes the wave travel in the $+z$ direction: toward the target for $z < 0$ and away from it for $z > 0$ [6].

A plane wave has definite energy and momentum along z, but it is *not* an eigenstate of $\boldsymbol{L}^2$. It is a coherent superposition of all orbital angular momenta. Because of axial symmetry about the beam, only projections $m = 0$ appear. The expansion in spherical waves (partial waves) reads

$$e^{ikz} = \sum_{\ell=0}^{\infty} i^{\ell}(2\ell+1)\, j_\ell(kr)\, P_\ell(\cos\theta), \tag{1.5}$$

where j_ℓ are spherical Bessel functions and P_ℓ Legendre polynomials. Each term $\ell = 0, 1, 2, \ldots$ is an s, p, d, … wave with a definite impact-parameter character in the semiclassical picture.

1.4 Phase shifts: what a short-range potential can do

Detectors sit centimetres from the target, while the nuclear force acts only for $r \lesssim$ a few fm. Outside the force range the wave is free again; the potential cannot change its wavelength there. What it *can* do is shift the phase of each outgoing partial wave relative to the free solution.

Free spherical waves have the asymptotic form

$$j_\ell(kr) \sim \frac{\sin(kr - \ell\pi/2)}{kr} \qquad (kr \to \infty). \tag{1.6}$$

In the presence of a short-range central potential the radial function $u_\ell(r) = rR_\ell(r)$ for r larger than the force range becomes

$$u_\ell(r) \sim \sin\big(kr - \ell\pi/2 + \delta_\ell\big), \tag{1.7}$$

where $\delta_\ell(E)$ is the **phase shift** in channel ℓ [6, 2]. Attractive potentials typically pull nodes of u_ℓ toward the origin (positive δ_ℓ); repulsive potentials push nodes outward (negative δ_ℓ).

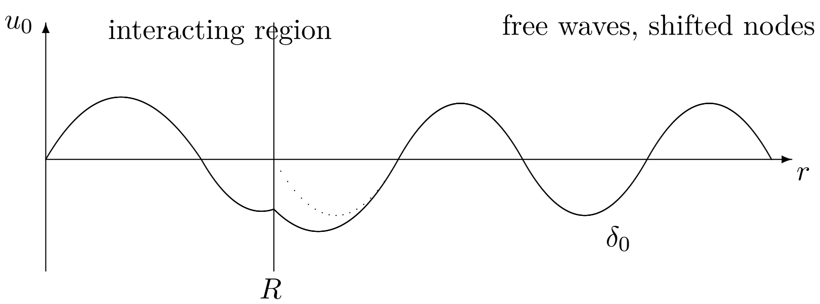

Figure 1.2: Schematic s-wave radial wave $u(r)$. Inside the force range the potential distorts the wave; outside, the free oscillation is shifted by the phase δ_0.

All information about $V(r)$ that elastic scattering at energy E can provide is encoded in the set $\{\delta_\ell(E)\}$. Solving the radial Schrödinger equation for a model potential and reading δ_ℓ is the theoretical route; measuring $\mathrm{d}\sigma/\mathrm{d}\Omega$ and fitting δ_ℓ is the experimental route. Phase shifts themselves are not directly observed: they are a convenient parameterisation of the measured cross sections (and polarisations). The two routes meet in (1.12) below.

For $\ell = 0$ one may write the exterior wave as a combination of incoming and outgoing spherical waves $e^{\pm ikr}/r$. Scattering does not create or destroy particles in elastic scattering, so it cannot change the *amplitudes* of those waves; it can only change the relative phase of the outgoing piece. That single phase is δ_0 (up to a conventional factor of two in intermediate steps of the algebra) [6].

1.4.1 Matching any partial wave at the force boundary

Let the potential vanish for $r > R$, and define the logarithmic derivative of the regular interior solution by

$$\mathcal{L}_\ell(E) = \left.\frac{u'_\ell}{u_\ell}\right|_R .$$

With Riccati–Bessel functions $\hat{j}_\ell(x) = xj_\ell(x)$ and $\hat{n}_\ell(x) = xn_\ell(x)$, write

$$u_\ell(r) = C_\ell \left[\hat{j}_\ell(kr)\cos\delta_\ell - \hat{n}_\ell(kr)\sin\delta_\ell\right].$$

Continuity of u_ℓ and u'_ℓ at R gives

$$\tan\delta_\ell = \frac{k\hat{j}'_\ell(kR) - \mathcal{L}_\ell \hat{j}_\ell(kR)}{k\hat{n}'_\ell(kR) - \mathcal{L}_\ell \hat{n}_\ell(kR)}. \tag{1.8}$$

Thus the interior radial equation supplies one logarithmic derivative, which fixes δ_ℓ, then S_ℓ, then the cross section.

1.5 Cross section from phase shifts

Matching the asymptotic partial-wave solution to an incident plane wave plus outgoing scattered spherical wave produces the scattering amplitude $f(\theta)$. Outside the force range the radial wave in channel ℓ may be written as a superposition of incoming and outgoing spherical waves,

$$u_\ell(r) \propto e^{-i(kr-\ell\pi/2)} - S_\ell\, e^{i(kr-\ell\pi/2)}, \tag{1.9}$$

with the unitary S-matrix element $S_\ell = e^{2i\delta_\ell}$ for a real central potential (elastic scattering). The coefficient of the outgoing scattered wave relative to the free case defines the partial-wave amplitude

$$f_\ell = \frac{S_\ell - 1}{2ik} = \frac{e^{2i\delta_\ell} - 1}{2ik} = \frac{e^{i\delta_\ell}\sin\delta_\ell}{k}. \tag{1.10}$$

The incoming and outgoing radial probability currents are proportional to their squared amplitudes. Elastic flux conservation therefore requires $|S_\ell| = 1$, so $S_\ell = e^{2i\delta_\ell}$ with real δ_ℓ. If inelastic channels open, one instead writes $S_\ell = \eta_\ell e^{2i\delta_\ell}$, $0 \le \eta_\ell < 1$; all formulae below use the elastic limit $\eta_\ell = 1$. Summing over partial waves with the Legendre weights of the plane-wave expansion gives

$$f(\theta) = \sum_{\ell=0}^{\infty}(2\ell+1)\, f_\ell\, P_\ell(\cos\theta) = \frac{1}{k}\sum_{\ell=0}^{\infty}(2\ell+1)\, e^{i\delta_\ell}\sin\delta_\ell\, P_\ell(\cos\theta). \tag{1.11}$$

The CM differential cross section is therefore

$$\frac{\mathrm{d}\sigma}{\mathrm{d}\Omega} = |f(\theta)|^2 = \frac{1}{k^2}\left|\sum_{\ell=0}^{\infty}(2\ell+1)\, e^{i\delta_\ell}\sin\delta_\ell\, P_\ell(\cos\theta)\right|^2. \tag{1.12}$$

(The overall phase convention for $e^{i\delta_\ell}$ varies among sources; the measurable $|f|^2$ is fixed by the δ_ℓ.) The factor $(2\ell+1)$ counts magnetic substates of a given ℓ; the Legendre polynomials build the angular pattern of each partial wave.

When only $\ell = 0$ contributes, $P_0 = 1$ and

$$\frac{\mathrm{d}\sigma}{\mathrm{d}\Omega} = \frac{\sin^2\delta_0}{k^2}, \tag{1.13}$$

independent of angle in the CM frame. For an s wave alone,

$$\sigma_{\mathrm{tot}} = \int \frac{\mathrm{d}\sigma}{\mathrm{d}\Omega}\,\mathrm{d}\Omega = \frac{\sin^2\delta_0}{k^2}\int \mathrm{d}\Omega = \frac{4\pi}{k^2}\sin^2\delta_0.$$

For a general partial-wave sum the different ℓ interfere in $\mathrm{d}\sigma/\mathrm{d}\Omega$, but after angular integration the cross terms vanish by orthogonality $\int P_\ell P_{\ell'}\,\mathrm{d}\Omega = 4\pi\delta_{\ell\ell'}/(2\ell+1)$. Each multipole then contributes separately:

$$\sigma_{\mathrm{tot}} = \frac{4\pi}{k^2}\sum_{\ell=0}^{\infty}(2\ell+1)\sin^2\delta_\ell = \frac{4\pi}{k^2}\sin^2\delta_0 \quad (s\text{-wave only}). \tag{1.14}$$

Thus a single number $\delta_0(E)$ determines the entire low-energy elastic yield. The unitarity bound $\sin^2\delta_0 \le 1$ implies $\sigma_{\mathrm{tot}} \le 4\pi/k^2$: at very low energy the quantum cross section can greatly exceed the geometric size of the potential well [6, 14].

Caution

Factor-of-four check. The physical outgoing-to-incoming phase is $S_\ell = e^{2i\delta_\ell}$, not $e^{i\delta_\ell}$. Hence

$$\left|\frac{S_\ell - 1}{2ik}\right|^2 = \frac{|2ie^{i\delta_\ell}\sin\delta_\ell|^2}{4k^2} = \frac{\sin^2\delta_\ell}{k^2}.$$

For an s wave this gives $\sigma_0 = 4\pi\sin^2\delta_0/k^2$. Dropping the factor 2 in $S - 1 = 2ie^{i\delta}\sin\delta$ produces the erroneous factor-of-four cross section.

1.5.1 Optical theorem from the same partial waves

At $\theta = 0$, $P_\ell(1) = 1$, and therefore

$$\mathrm{Im}\, f(0) = \frac{1}{k}\sum_{\ell=0}^{\infty}(2\ell+1)\sin^2\delta_\ell.$$

Comparison with Equation (1.14) yields

$$\boxed{\sigma_{\text{tot}} = \frac{4\pi}{k}\,\text{Im}\, f(0)}. \tag{1.15}$$

The optical theorem is therefore the forward-angle statement of partial-wave unitarity.

For equal-mass np scattering the laboratory and CM scattering angles are related by $\theta_{\text{lab}} = \theta_{\text{CM}}/2$, and

$$\left(\frac{\mathrm{d}\sigma}{\mathrm{d}\Omega}\right)_{\text{lab}} = 4\cos\theta_{\text{lab}}\left(\frac{\mathrm{d}\sigma}{\mathrm{d}\Omega}\right)_{\text{CM}}. \tag{1.16}$$

Partial-wave formulae in this lecture are always in the CM frame unless stated otherwise.

Key idea

Phase shifts δ_ℓ are the interface between potential and data. Theory: solve the radial equation for $V(r)$ and extract δ_ℓ. Experiment: measure $\mathrm{d}\sigma/\mathrm{d}\Omega$ and determine δ_ℓ.

1.6 Low energy: only s-wave scattering

Semiclassically, a projectile of momentum $p = \sqrt{2\mu E}$ that grazes the force range r_0 carries angular momentum $\ell\hbar \sim pr_0$. For nuclear $r_0 \sim 2\,\text{fm}$ and $E \sim 1\,\text{MeV}$ one finds $pr_0/\hbar \ll 1$: the projectile cannot bring $\ell \geq 1$ inside the nuclear force range without flying past outside the well. Only $\ell = 0$ scatters. At $E \sim 10\,\text{MeV}$, $\ell = 1$ begins to contribute [6].

A sharper estimate uses the free kinetic energy scale associated with confinement in a well of size R,

$$T \sim \frac{\ell(\ell+1)\hbar^2}{2\mu R^2}.$$

For $\ell = 1$, $R \sim 1\,\text{fm}$, and $\mu c^2 \sim 500\,\text{MeV}$, T is tens of MeV. Incident energies far below that scale justify the s-wave truncation [6].

This is why low-energy np data are so powerful and so simple: a single phase $\delta_0(E)$ (actually one for each spin channel) carries the dynamics, and $\sigma(\theta)$ is nearly isotropic.

1.7 Square well in the continuum: matching for $E > 0$

The same square well used for the deuteron bound state can be solved for positive energy. For $\ell = 0$,

$$V(r) = \begin{cases} -V_0 & r < R, \\ 0 & r > R, \end{cases} \qquad E > 0. \tag{1.17}$$

Inside, $u(r) = A\sin(k_1 r)$ with $k_1 = \sqrt{2\mu(V_0 + E)}/\hbar$ (regularity at the origin again kills the cosine). Outside,

$$u(r) = C\sin(kr + \delta_0), \qquad k = \frac{\sqrt{2\mu E}}{\hbar}. \tag{1.18}$$

Continuity of u and u' at $r = R$ yields

$$k\cot(kR + \delta_0) = k_1\cot(k_1 R). \tag{1.19}$$

Solving for the phase shift,

$$\delta_0 = \arctan\!\left(\frac{k}{k_1}\tan(k_1 R)\right) - kR \pmod{\pi}. \tag{1.20}$$

Given E, V_0, and R, one thus obtains $\delta_0(E)$ and then predicts σ_{tot} from (1.14) [6].

In the zero-energy limit $k \to 0$, $k_1 \to K \equiv \sqrt{2\mu V_0}/\hbar$ and the scattering length extracted from $a = -\lim(\tan\delta_0/k)$ becomes

$$a = R - \frac{\tan(KR)}{K}. \tag{1.21}$$

(If $KR = \pi/2$, $a \to \infty$: the zero-energy bound-state threshold of Lecture 7.) Then $\sigma_{\text{tot}} \to 4\pi a^2$.

As $V_0 \to 0$, $\delta_0 \to 0$ and there is no scattering. For the attractive well fitted to the deuteron ($V_0 \approx 35\,\text{MeV}$, $R \sim 2\,\text{fm}$), low-energy δ_0 is large and σ_{tot} is tens of barns. Experiment finds the zero-energy unpolarised np cross section near 20 b, not the $\sim$ 4–5 b that a pure triplet estimate would suggest. The resolution is that free protons and neutrons scatter in a statistical mixture of triplet and singlet spins: three triplet states and one singlet, so the spin weights are 3/4 and 1/4. Writing

$$\sigma = \tfrac{3}{4}\sigma_t + \tfrac{1}{4}\sigma_s, \tag{1.22}$$

and taking $\sigma_t \approx 4\pi a_t^2 \sim 4.6\,\text{b}$ from the deuteron (triplet) channel leaves $\sigma_s \sim 70\,\text{b}$: the singlet interaction is strong but just unbound, producing a large negative scattering length [6, 14].

1.8 Scattering length and effective range

At vanishing energy, $\delta_0 \to 0$ in such a way that

$$a = -\lim_{k\to 0}\frac{\tan\delta_0}{k} \tag{1.23}$$

defines the **scattering length** a. At low energy $\delta_0 \to 0$ with $\tan\delta_0 \sim \delta_0 \sim \sin\delta_0$, so

$$\tan\delta_0 \approx -ka \quad\Rightarrow\quad \sin\delta_0 \approx -ka$$

(to leading order in k). Insert into the s-wave total cross section:

$$\sigma_{\text{tot}} = \frac{4\pi}{k^2}\sin^2\delta_0 \approx \frac{4\pi}{k^2}(ka)^2 = 4\pi a^2. \tag{1.24}$$

Thus as $k \to 0$,

$$\sigma_{\text{tot}} \to 4\pi a^2. \tag{1.25}$$

The sign of a carries physics: a large *positive* scattering length is characteristic of a barely bound state (triplet, deuteron); a large *negative* scattering length signals a virtual state just above threshold (singlet) [6, 14].

Checked low-energy np numbers

Standard values are $a_t \approx +5.4\,\mathrm{fm}$ (triplet) and $a_s \approx -23.7\,\mathrm{fm}$ (singlet). The unpolarised zero-energy cross section is then

$$\begin{aligned}\sigma &= 4\pi\left(\tfrac{3}{4}a_t^2 + \tfrac{1}{4}a_s^2\right)\\ &= 4\pi\left(\tfrac{3}{4}(5.4)^2 + \tfrac{1}{4}(23.7)^2\right) \approx 4\pi(21.9 + 140.4) \approx 20\,\mathrm{b},\end{aligned}$$

matching experiment. The huge singlet piece dominates because $|a_s|$ is so large: the singlet potential nearly binds [6, 14].

A more accurate low-energy expansion follows from matching the exterior wave to an effective-range expansion of the logarithmic derivative. Writing

$$k\cot\delta_0 = -\frac{1}{a} + \frac{1}{2}r_0k^2 + \cdots\,, \tag{1.26}$$

defines the effective range r_0 of fermi size. The first two terms already reproduce low-energy $\delta_0(E)$ in each spin channel without committing to a full potential at every energy [6, 14]. Fitting a and r_0 is how modern analyses encode low-energy NN physics.

The s-wave amplitude itself is

$$f_0(k) = \frac{1}{k\cot\delta_0 - ik} = \frac{1}{-1/a + \frac{1}{2}r_0k^2 - ik + \cdots}. \tag{1.27}$$

This form exposes both unitarity (the $-ik$ term) and the pole structure. A shallow bound state is a pole at $k = i\kappa$, $\kappa > 0$. Setting the denominator to zero,

$$-\frac{1}{a} + \frac{1}{2}r_0(-\kappa^2) - i(i\kappa) = 0 \quad \Rightarrow \quad -\frac{1}{a} - \frac{1}{2}r_0\kappa^2 + \kappa = 0, \tag{1.28}$$

so

$$\frac{1}{a} = \kappa - \frac{1}{2}r_0\kappa^2 + \cdots\,. \tag{1.29}$$

At leading order $a \simeq 1/\kappa > 0$, as in the triplet deuteron channel. A pole on the negative imaginary axis is a virtual state and corresponds at leading order to a large negative a, as in the singlet channel. For the square well, $KR = \pi/2$ makes $a = R - \tan(KR)/K$ diverge: the pole reaches zero energy at exactly the bound-state threshold found in Lecture 7.

Key idea

The deuteron fixes the *triplet* well near threshold. Scattering reveals a strong *singlet* interaction that fails to bind, and it maps how $\delta_\ell(E)$ evolve as higher partial waves open with energy.

1.9 Deeper physics: partial waves, scattering length, and unitarity

1.9.1 From plane wave to partial-wave cross section

The lecture expands a plane wave in partial waves (Equation (1.5)) and shows that a short-range potential can only shift the phase of each outgoing channel (Equation (1.7)). The differential cross section then becomes a sum over ℓ:

$$\frac{d\sigma}{d\Omega} = \frac{1}{k^2}\left|\sum_{\ell=0}^{\infty}(2\ell+1)\,e^{i\delta_\ell}\,\sin\delta_\ell\,P_\ell(\cos\theta)\right|^2, \tag{1.30}$$

which is (1.12) in the main text. At low energy only $\ell = 0$ contributes (the centrifugal barrier $\sim \ell(\ell+1)/r^2$ suppresses higher waves), so the angular distribution is isotropic and fixing $\delta_0(E)$ fixes the entire cross section.

1.9.2 Scattering length and effective range

Expanding $\delta_0(E) \approx -ka + \mathcal{O}(k^3)$ defines the **scattering length** a (Equation (1.23)). For the np triplet channel, $a_t \approx +5.4\,\text{fm}$: the interaction is weakly attractive at threshold, consistent with a shallow bound state (the deuteron, Lecture 7). The next term in the low-energy expansion defines the **effective range** r_e (Equation (1.26)), which sets the curvature of $\delta_0(E)$ and is linked to the interior shape of $V(r)$. Together (a, r_e) are the minimal low-energy data for each spin channel; they cannot be read from B_d alone.

Geometric cross section at nuclear size

For a black-disk target of radius $R \approx 1.2\,A^{1/3}\,\text{fm}$,

$$\sigma_{\text{geo}} = \pi R^2 \approx \begin{cases} 45\,\text{mb} & A = 12, \\ 1.3\,\text{b} & A = 208, \end{cases} \tag{1.31}$$

using $1\,\text{b} = 100\,\text{mb}$. Measured total reaction cross sections at tens of MeV often approach this geometric scale, while elastic NN cross sections at low energy are set instead by a^2 because the force range is only a few fm [6, 2].

1.9.3 Optical theorem as a consistency check

The optical theorem (Equation (1.15)) ties the forward amplitude to the total cross section:

$$\sigma_{\text{tot}} = \frac{4\pi}{k}\,\Im f(0). \tag{1.32}$$

In partial-wave language, $\sigma_{\text{tot}} = (4\pi/k)\sum_\ell(2\ell+1)\sin^2\delta_\ell$. Each δ_ℓ must be real for elastic scattering, so the sum is automatically positive: unitarity is built in. When imaginary optical potentials are introduced for heavy-ion reactions (absorption into other channels), δ_ℓ acquires an imaginary part and the same relation remains the bookkeeping check that flux removed from the elastic channel equals flux into all inelastic channels.

1.9.4 Levinson's theorem and the deuteron pole

For a short-range central potential with one s-wave bound state, Levinson's theorem states $\delta_0(E = 0) = +\pi/2$. The scattering length is then positive and large when the bound state is weakly bound ($a \gg R$). The deuteron pole in the T-matrix at $E = -B_d$ is the analytic continuation of this phase-shift behaviour: scattering and bound-state data are linked, not independent fits [6, 2]. Lecture 7's square well sits at the same threshold; Lecture 11's Yukawa tail sets the slope of $\delta_0(E)$ at higher energy through r_e.

1.9.5 When partial waves beyond $\ell = 0$ matter

At centre-of-mass energy $E \sim 50\,\text{MeV}$, the p-wave ($\ell = 1$) channel opens with centrifugal barrier $\hbar^2\ell(\ell+1)/(2\mu r^2)$ suppressing low-r penetration. Triplet p waves and tensor mixing of s and d waves become comparable in importance. At low energy ($E \lesssim 10\,\text{MeV}$), however, the story collapses to real δ_0 and the isotropic cross section (1.33), which is why hydrogen-target neutron scattering at thermal energies isolates the singlet/triplet spin structure introduced in Lecture 7.

1.10 Further physics: coherent scattering and spin channels

At very low energy the de Broglie wavelength of a neutron can exceed the size of a hydrogen molecule. Scattering from the two protons then interferes coherently, and the cross sections of ortho- and parahydrogen differ because the total proton spin of the molecule weights triplet and singlet np amplitudes differently. That difference is direct evidence that $\sigma_t \neq \sigma_s$ [6].

The optical analogy remains useful: an attractive well of nuclear size diffracts the incident wave much as an obstacle of size R diffracts light of wavelength $\lambda \sim 2\pi/k$. Partial-wave analysis is the quantum bookkeeping of that diffraction pattern, partial wave by partial wave.

1.10.1 Source-map limitation

No text file named `Lecture10_raw.txt` was present in the supplied course archive when this chapter was remediated. Consequently, statements cannot be mapped line-by-line to an original Lecture 10 raw transcript. The derivations are instead checked against the existing cited textbook keys, and every redrawn figure has an explicit record in the relevant `SOURCES.txt`. This documents the gap rather than inventing a raw provenance.

1.10.2 Low-energy s-wave cross section

When only $\ell = 0$ contributes, (1.12) reduces to

$$\sigma_{\text{tot}} = \frac{4\pi}{k^2}\sin^2\delta_0 \approx 4\pi a^2 \qquad (k \to 0), \tag{1.33}$$

using $\delta_0 \approx -ka$. For np scattering in the triplet channel, $a_t \approx +5.4\,\text{fm}$ gives $\sigma_t \approx 4\pi a_t^2 \approx 0.37\,\text{b}$, while the singlet channel with $a_s \approx -23.7\,\text{fm}$ yields $\sigma_s \approx 7\,\text{b}$. The dramatic difference between spin channels is direct evidence of the spin-dependent force introduced phenomenologically in Lecture 7's two-well picture [6, 14].

1.10.3 Effective range and the interior of $V(r)$

The effective-range expansion (Equation (1.26))

$$k\cot\delta_0 = -\frac{1}{a} + \frac{1}{2}r_e k^2 + \cdots \tag{1.34}$$

connects the curvature of $\delta_0(E)$ at threshold to the rms extent of the interaction region. For the triplet channel, $r_{e,t} \approx 1.7\,\mathrm{fm}$, comparable to the deuteron size. The deuteron binding energy fixes the *slope* of $k\cot\delta_0$ near $E = 0$ (Levinson's theorem links one bound state to a $\pi/2$ phase shift at threshold), but r_e carries independent information about the potential shape inside $r \lesssim 2\,\mathrm{fm}$. Fitting both a and r_e breaks the (R, V_0) degeneracy of the square well (Lecture 7 further material).

Optical theorem at $E = 50\,\mathrm{MeV}$

For np scattering near $50\,\mathrm{MeV}$, several partial waves contribute and $\sigma_{\mathrm{tot}} \sim 50$–$100\,\mathrm{mb}$. The optical theorem (Equation (1.15)) requires that the forward scattering amplitude's imaginary part reproduce this total. At higher energy, the geometric scale πR^2 with $R \sim 1\,\mathrm{fm}$ gives $\sim 10\,\mathrm{mb}$ per nucleon–nucleon collision, while heavy-ion reaction cross sections grow with $A^{2/3}$ (Lecture 10 main text, Equation (1.3)).

1.10.4 Bridge to Lecture 11 and the deuteron

Yukawa potentials with range $\hbar/(m_\pi c)$ generate phase shifts that can be fitted to (a, r_e) in each spin channel (Lecture 11). The deuteron (Lectures 7–9) is the bound-state pole in the triplet s-wave amplitude (Equation (1.29)): scattering and bound-state data are two views of the same T-matrix. Tensor and spin–orbit terms mix partial waves at higher ℓ, but at low energy the story reduces to real δ_0 and the unitarity sum in (1.33) [2, 6].

1.10.5 Coherent scattering from parahydrogen

When the neutron wavelength exceeds the H_2 bond length, scattering from the two protons adds coherently. Parahydrogen ($I_{\mathrm{mol}} = 0$) weights the singlet np channel; orthohydrogen ($I_{\mathrm{mol}} = 1$) weights the triplet. The measured difference in total cross sections at $E \lesssim 0.1\,\mathrm{eV}$ directly confirms $\sigma_t \neq \sigma_s$ without resolving individual phase shifts. That experiment is historically important because it established spin-dependent NN forces before direct accelerator phase-shift analyses [6, 14].

1.10.6 Partial-wave unitarity and the $\ell = 1$ turn-on

As energy increases, the $\ell = 1$ partial wave turns on when $kR_{\mathrm{eff}} \sim 1$. For $A = 12$ targets at $E \sim 20\,\mathrm{MeV}$, several partial waves contribute and diffraction minima appear in $\mathrm{d}\sigma/\mathrm{d}\Omega$. The optical theorem (Equation (1.15)) still holds channel by channel: the imaginary part of each partial-wave amplitude fixes the contribution to σ_{tot}. For NN scattering at low energy the unitarity sum collapses to $\sin^2\delta_0$, linking the deuteron pole (Lecture 7) to the threshold cross sections quoted in (1.33) [2, 6].

1.11 Deeper reading: unitarity, optical theorem, and optical potentials

At unitarity, an S-wave cross section saturates $\sigma = 4\pi/k^2$. Low-energy np scattering is large because the deuteron is near threshold, not because the force is singular in a naive sense. The optical theorem links $\operatorname{Im} f(0)$ to the total cross section and thereby constrains absorptive (imaginary) potentials once inelastic channels open.

$$\sigma_{\text{tot}} = \frac{4\pi}{k}\operatorname{Im} f(\theta = 0). \tag{1.35}$$

Optical potentials used in Lecture 21 reactions are the many-body descendants of this idea: a complex mean field that reproduces elastic scattering while accounting for absorption into other channels. Uncertainty quantification of those potentials is now part of extracting spectroscopic factors. Partial-wave analyses of NN scattering remain the calibration point for the chiral forces of Lecture 11 and for the few-body calculations that start from the deuteron (Lectures 7–9).

Coulomb versus nuclear phases

In charged-particle scattering, Coulomb phases multiply nuclear partial wave amplitudes. Extracting nuclear phase shifts therefore requires a careful Coulomb subtraction, especially at low energy and high Z. Neutron scattering avoids that complication and historically fixed much of the low-energy NN database.

Optical potential uncertainties

When an optical potential is fitted to elastic angular distributions, imaginary depths are constrained by absorption, real depths by refractive patterns and rainbows. Propagating the fit covariance into a transfer calculation is now expected practice. A spectroscopic factor quoted to three digits without an optical-model error bar is incomplete.

Worked unitarity and effective-range numbers

At $E_{\text{lab}} = 1\,\text{keV}$ for np, k is tiny and $\sigma \approx 4\pi a^2$ with a of several femtometres yields tens of barns: huge compared with πR^2 for a nucleus. That enhancement is threshold physics, not a failure of geometry. Adding the effective-range term $-\frac{1}{2}r_e k^2$ in $k\cot\delta_0$ curves the cross section upward in energy; fitting both a and r_e is the minimal data-driven model before introducing a potential shape.

For charged projectiles, replace the discussion with Coulomb-modified scattering lengths. The important conceptual transfer to Lecture 21 is that reaction theory inherits these low-energy constants when it uses NN potentials or optical models constrained by elastic data. Always ask which elastic database and which energy range constrained the interaction behind a published transfer calculation.

Scattering theory supplies the boundary conditions of nuclear reactions. Partial waves, scattering lengths, and optical potentials are not a side topic; they are the entrance channel to Lectures 21–22.

In practice, rework one numerical estimate from the lecture with a different parameter set and compare the shift to the quoted experimental uncertainty. If the shift exceeds the uncertainty, the estimate is teaching a scale, not delivering a fit. That distinction keeps theoretical cartoons honest when they sit beside evaluated data tables and modern many-body calculations. Along the course arc, write one sentence linking this chapter backward and one forward: the discipline of those two sentences is as important as any single formula. Examination problems rarely ask for a literature review, but they do ask for the scale argument that literature reviews presuppose.

Synthesis problem

Write a half-page note that (i) restates the chapter's central scale or selection rule in one equation, (ii) evaluates it numerically for one concrete nucleus or energy, and (iii) names the neighbouring lecture that uses the result. Keep the note free of research-frontier speculation; the goal is fluency with the lecture physics itself. If an assumption fails (Born approximation, spherical mean field, allowed transition, one-dimensional barrier), state the failure mode in a final sentence. That habit converts passive reading into examination-ready understanding and makes the later research-frontier box read as an extension rather than a replacement.

Research frontier: scattering with uncertainty quantification and student projects

Partial-wave analysis and optical potentials of Lecture 10 are being rebuilt with quantified uncertainties. Bayesian fits of nucleon–nucleon phase shifts, optical-model parameters with posterior predictive distributions, and EFT-based interactions embedded in reaction frameworks replace older point estimates that quoted only best-fit χ^2 [42, 41]. Rare-isotope beams demand reaction theories that treat breakup, continuum coupling, and target excitation on equal footing with structure, because spectroscopic factors extracted without those couplings can be misleading [51]. R-matrix methods remain central for resonance analyses in light systems, but modern implementations emphasise consistent channel truncations and covariance of resonance parameters. Uncertainties that still limit many applications include the imaginary (absorptive) part of optical potentials for exotic projectiles and the propagation of interaction uncertainties into transfer and knockout cross sections.

For radioactive beams, the optical potential is often underconstrained because elastic data are sparse. Uncertainty quantification then becomes part of the structure extraction: a spectroscopic factor quoted without an optical-model error bar is incomplete. Learning to read covariance bands on angular distributions is therefore a modern experimental-theory skill.

Reporting a spectroscopic factor together with an optical-model error band is now expected practice in rare-isotope reaction papers.

That habit of quoting covariances alongside central values is the main cultural shift relative to older optical-model papers.

Student directions. (1) Data exercise: from a published S-wave phase shift, reconstruct the scattering length and effective range. (2) Scale estimate: compute the geometric $\sigma = \pi R^2$ scale for $A = 12$ and $A = 208$ and compare with measured reaction cross sections at one energy. (3) Methods outline: explain how an optical-model imaginary depth is constrained by elastic angular distributions.

1.12 Problems with solutions

Problem 10.1 — Cross section dimensions

From $\mathrm{d}N = \sigma\, t\, \mathrm{d}\Omega\, I\, N_t$, show that σ has dimensions of area.

Solution 10.1

$\mathrm{d}N$ is dimensionless (a count). tI has dimensions of (time)$\times$(area^{-1} time^{-1})=area^{-1}; N_t is a number; $\mathrm{d}\Omega$ is dimensionless. Hence σ must supply an area so that the product is dimensionless.

Problem 10.2 — Low-energy total cross section

At low energy only δ_0 is nonzero. Show that $\sigma_{\text{tot}} = 4\pi k^{-2} \sin^2 \delta_0$. If $\delta_0 = \pi/2$, what is σ_{tot}?

Solution 10.2

From $f = (e^{i\delta_0} \sin \delta_0)/k$ one has $\mathrm{d}\sigma/\mathrm{d}\Omega = |f|^2 = \sin^2 \delta_0/k^2$, isotropic in the CM frame. Integrate:

$$\sigma_{\text{tot}} = \int \frac{\sin^2 \delta_0}{k^2}\, \mathrm{d}\Omega = \frac{4\pi}{k^2} \sin^2 \delta_0.$$

At resonance-like $\delta_0 = \pi/2$, $\sigma_{\text{tot}} = 4\pi/k^2$ (unitarity limit for s-wave) [6].

Problem 10.3 — Why only s-wave at $1\,\text{MeV}$

Estimate $\ell_{\max} \sim p r_0/\hbar$ for $E = 1\,\text{MeV}$ (lab-scale NN), $r_0 = 2\,\text{fm}$, $\hbar c = 200\,\text{MeV fm}$, $\mu c^2 \approx 500\,\text{MeV}$. Argue that $\ell = 0$ dominates.

Solution 10.3

$$pc = \sqrt{2\mu c^2\, E} \approx \sqrt{1000\,\text{MeV}^2} \approx 32\,\text{MeV}, \qquad \frac{p r_0}{\hbar} = \frac{(pc)\, r_0}{\hbar c} \approx \frac{32 \times 2}{200} \approx 0.3.$$

Values $\ell \geq 1$ require order-1 or larger; only $\ell = 0$ fits inside the nuclear range at this energy [6].

Problem 10.4 — Square-well matching and threshold

For the s-wave square well, match $u_{\text{in}} = A\sin(k_1 r)$ to $u_{\text{out}} = C\sin(kr + \delta_0)$ at R. Derive $k\cot(kR + \delta_0) = k_1 \cot(k_1 R)$, obtain the zero-energy scattering length, and identify the first bound-state threshold.

Solution 10.4

Continuity of u and u', followed by division, gives

$$k_1 \cot(k_1 R) = k\cot(kR + \delta_0).$$

As $k \to 0$, the exterior zero-energy form is proportional to $r - a$. Matching its logarithmic derivative to the interior one, with $K = \sqrt{2\mu V_0}/\hbar$, yields

$$a = R - \frac{\tan(KR)}{K}.$$

The first divergence occurs at $KR = \pi/2$, or $V_0 R^2 = \pi^2\hbar^2/(8\mu)$, exactly the first bound-state threshold.

Problem 10.5 — Unitarity and optical theorem

Starting with $S_\ell = e^{2i\delta_\ell}$, show that $f_\ell = (S_\ell - 1)/(2ik) = e^{i\delta_\ell}\sin\delta_\ell/k$. Then derive the optical theorem from the partial-wave expansion.

Solution 10.5

The identity $e^{2i\delta} - 1 = 2ie^{i\delta}\sin\delta$ gives the stated amplitude and ensures the correct factor of four in $\sigma_\ell = 4\pi(2\ell+1)\sin^2\delta_\ell/k^2$. At zero angle,

$$\operatorname{Im} f(0) = \frac{1}{k}\sum_\ell (2\ell+1)\sin^2\delta_\ell.$$

Multiplication by $4\pi/k$ reproduces the summed total cross section:

$$\sigma_{\text{tot}} = \frac{4\pi}{k}\operatorname{Im} f(0).$$

Problem 10.6 — Effective-range pole check

Insert $k = i\kappa$ into

$$f_0(k) = \frac{1}{-1/a + \frac{1}{2}r_0 k^2 - ik}$$

and derive the shallow-bound-state pole condition. Explain the signs of the triplet and singlet scattering lengths.

Solution 10.6

At $k = i\kappa$, the denominator vanishes when

$$-\frac{1}{a} - \frac{1}{2}r_0\kappa^2 + \kappa = 0, \qquad \frac{1}{a} = \kappa - \frac{1}{2}r_0\kappa^2.$$

Thus a shallow physical bound state has $a > 0$ at leading order, matching the triplet deuteron channel. A virtual-state pole on the negative imaginary axis gives a large negative a, matching the unbound singlet channel.

Bibliography

[1] R. A. Dunlap, *An Introduction to the Physics of Nuclei and Particles* (2nd ed.), IOP Publishing, Bristol (2023), DOI: 10.1088/978-0-7503-6094-4, Ch. 3 (Nuclear composition and size).

[2] W. Demtröder, *Nuclear and Particle Physics*, Undergraduate Lecture Notes in Physics, Springer, Cham (2023).

[3] S. Petrera, *Problems and Solutions in Nuclear and Particle Physics*, UNITEXT for Physics, Springer, Cham (2019).

[4] F. Terranova, *A Modern Primer in Particle and Nuclear Physics*, Oxford University Press (2021).

[5] S. D'Auria, *Introduction to Nuclear and Particle Physics*, Undergraduate Lecture Notes in Physics, Springer, Cham (2018).

[6] K. S. Krane, *Introductory Nuclear Physics*, Wiley, New York (1988).

[7] R. Hofstadter, "Electron scattering and nuclear structure," Rev. Mod. Phys. **28**, 214 (1956).

[8] H. F. Ehrenberg, R. Hofstadter, U. Meyer-Berkhout, D. G. Ravenhall, and S. E. Sobottka, "High-Energy Electron Scattering and the Charge Distribution of Carbon-12 and Oxygen-16," Phys. Rev. **113**, 666 (1959).

[9] H. Yukawa, "On the interaction of elementary particles. I," Proc. Phys.-Math. Soc. Japan **17**, 48 (1935).

[10] R. D. Woods and D. S. Saxon, "Diffuse surface optical model for nucleon-nuclei scattering," Phys. Rev. **95**, 577 (1954).

[11] H. G. J. Moseley, "The high-frequency spectra of the elements," Phil. Mag. **26**, 1024 (1913); **27**, 703 (1914).

[12] C. F. von Weizsäcker, "Zur Theorie der Kernmassen," Z. Phys. **96**, 431 (1935).

[13] P. Cappellaro, *Introduction to Applied Nuclear Physics* (MIT OpenCourseWare / LibreTexts), CC BY-NC-SA 4.0.

[14] J.-L. Basdevant, J. Rich, and M. Spiro, *Fundamentals in Nuclear Physics: From Nuclear Structure to Cosmology*, Springer, New York (2005).

[15] D. Tong, *Particle Physics*, Lecture notes (University of Cambridge / CERN school notes).

[16] M. G. Mayer, "On closed shells in nuclei. II," Phys. Rev. **75**, 1969 (1949).

[17] O. Haxel, J. H. D. Jensen, and H. E. Suess, "On the "magic numbers" in nuclear structure," Phys. Rev. **75**, 1766 (1949).

[18] T. Schmidt, "Über die magnetischen Momente der Atomkerne," Z. Phys. **106**, 358 (1937).

[19] L. W. Nordheim, "On spins, moments, and shells in nuclei," Phys. Rev. **78**, 294 (1950).

[20] Evaluated Nuclear Structure Data File (ENSDF), National Nuclear Data Center, Brookhaven National Laboratory, `https://www.nndc.bnl.gov/ensdf/`.

[21] NuDat 3, National Nuclear Data Center, Brookhaven National Laboratory, `https://www.nndc.bnl.gov/nudat3/`.

[22] N. J. Stone, "Table of nuclear magnetic dipole and electric quadrupole moments," At. Data Nucl. Data Tables **90**, 75 (2005); updated compilations at NNDC.

[23] W. N. Cottingham and D. A. Greenwood, *An Introduction to Nuclear Physics* (2nd ed.), Cambridge University Press, Cambridge (2001).

[24] H. Geiger and J. M. Nuttall, "The ranges of the α particles from the radioactive substances," Phil. Mag. **22**, 613 (1911).

[25] G. Gamow, "Zur Quantentheorie des Atomkernes," Z. Phys. **51**, 204 (1928).

[26] R. W. Gurney and E. U. Condon, "Wave mechanics and radioactive disintegration," Nature **122**, 439 (1928); Phys. Rev. **33**, 127 (1929).

[27] M. Wang, W. J. Huang, F. G. Kondev, G. Audi, and S. Naimi, "The AME 2020 atomic mass evaluation (II). Tables, graphs and references," Chin. Phys. C **45**, 030003 (2021).

[28] Laboratoire National Henri Becquerel (LNHB), Recommended decay data, `http://www.lnhb.fr/nuclear-data/nuclear-data-table/`.

[29] L. M. Langer, R. D. Moffat, and H. C. Price, Jr., "Low energy beta-ray spectra: P^{32} and Cu^{64}," Phys. Rev. **76**, 1725 (1949).

[30] L. M. Langer and H. C. Price, Jr., "Shapes of the beta-spectra of the forbidden transitions of Sb^{124}, Rb^{86}, Sr^{89}, Y^{91}, and Cs^{137}," Phys. Rev. **75**, 1769 (1949).

[31] D. C. Camp and L. M. Langer, "The shape of the ^{66}Ga positron spectrum and the contribution from $0^+ \to 0^+$ transitions," Phys. Rev. **129**, 1782 (1963).

[32] H. C. Verma, *Nuclear Physics: Fundamentals and Applications*, NPTEL/IIT Kanpur lecture series, `https://hcverma.in/ncl_phy_lectures`.

[33] International Atomic Energy Agency, *LiveChart of Nuclides*, evaluated structure, decay, reaction, and fission-yield data, `https://www-nds.iaea.org/relnsd/vcharthtml/VChartHTML.html`.

[34] T. Kibédi, T. W. Burrows, M. B. Trzhaskovskaya, P. M. Davidson, and C. W. Nestor, Jr., "Evaluation of theoretical conversion coefficients using BrIcc," Nucl. Instrum. Methods Phys. Res. A **589**, 202 (2008), DOI: 10.1016/j.nima.2008.02.051.

[35] D. A. Brown *et al.*, "ENDF/B-VIII.0: The 8th major release of the nuclear reaction data library with CIELO-project cross sections, new standards and thermal scattering data," Nucl. Data Sheets **148**, 1 (2018), DOI: 10.1016/j.nds.2018.02.001.

[36] B. Acharya *et al.*, "Solar fusion III: New data and theory for hydrogen-burning stars," Rev. Mod. Phys. **97**, 035002 (2025), DOI: 10.1103/8lm7-gs18.

[37] S. N. Ghoshal, "An experimental verification of the theory of compound nucleus," Phys. Rev. **80**, 939 (1950), DOI: 10.1103/PhysRev.80.939.

[38] D. Adhikari *et al.* (PREX Collaboration), "Accurate determination of the neutron skin thickness of ^{208}Pb through parity-violation in electron scattering," Phys. Rev. Lett. **126**, 172502 (2021), DOI: 10.1103/PhysRevLett.126.172502.

[39] B. T. Reed, F. J. Fattoyev, C. J. Horowitz, and J. Piekarewicz, "Implications of PREX-II on the equation of state of neutron-rich matter," Phys. Rev. Lett. **126**, 172503 (2021), DOI: 10.1103/PhysRevLett.126.172503.

[40] B. Hu *et al.*, "Ab initio predictions link the neutron skin of ^{208}Pb to nuclear forces," Nature Phys. **18**, 1196 (2022), DOI: 10.1038/s41567-022-01715-8.

[41] E. Epelbaum, H.-W. Hammer, and U.-G. Meißner, "Modern theory of nuclear forces," Rev. Mod. Phys. **81**, 1773 (2009), DOI: 10.1103/RevModPhys.81.1773.

[42] H.-W. Hammer, S. König, and U. van Kolck, "Nuclear effective field theory: Status and perspectives," Rev. Mod. Phys. **92**, 025004 (2020), DOI: 10.1103/RevModPhys.92.025004.

[43] T. Otsuka, A. Gade, O. Sorlin, T. Suzuki, and Y. Utsuno, "Evolution of shell structure in exotic nuclei," Rev. Mod. Phys. **92**, 015002 (2020), DOI: 10.1103/RevModPhys.92.015002.

[44] H. Hergert, S. K. Bogner, T. D. Morris, A. Schwenk, and K. Tsukiyama, "The in-medium similarity renormalization group: A novel ab initio method for nuclei," Phys. Rep. **621**, 165 (2016), DOI: 10.1016/j.physrep.2015.12.007.

[45] J. M. Lattimer and M. Prakash, "The equation of state of hot, dense matter and neutron stars," Phys. Rep. **621**, 127 (2016), DOI: 10.1016/j.physrep.2015.12.005.

[46] J. M. Lattimer, "Neutron stars and the nuclear matter equation of state," Annu. Rev. Nucl. Part. Sci. **71**, 433 (2021), DOI: 10.1146/annurev-nucl-102419-124827.

[47] B. P. Abbott *et al.* (LIGO Scientific Collaboration and Virgo Collaboration), "GW170817: Observation of gravitational waves from a binary neutron star inspiral," Phys. Rev. Lett. **119**, 161101 (2017), DOI: 10.1103/PhysRevLett.119.161101.

[48] M. J. Dolinski, A. W. P. Poon, and W. Rodejohann, "Neutrinoless double-beta decay: Status and prospects," Annu. Rev. Nucl. Part. Sci. **69**, 219 (2019), DOI: 10.1146/annurev-nucl-101918-023407.

[49] M. Agostini, G. Benato, J. A. Detwiler, J. Menéndez, and F. Vissani, "Toward the discovery of matter creation with neutrinoless $\beta\beta$ decay," Rev. Mod. Phys. **95**, 025002 (2023), DOI: 10.1103/RevModPhys.95.025002.

[50] P. Gysbers *et al.*, "Discrepancy between experimental and theoretical β-decay rates resolved from first principles," Nature Phys. **15**, 428 (2019), DOI: 10.1038/s41567-019-0450-7.

[51] H. L. Crawford, K. Fossez, S. König, and A. Spyrou, "A vision for the science of rare isotopes," Annu. Rev. Nucl. Part. Sci. **74**, 141 (2024), DOI: 10.1146/annurev-nucl-121423-091501.

[52] Nuclear Science Advisory Committee, *A New Era of Discovery: The 2023 Long Range Plan for Nuclear Science*, U.S. Department of Energy and National Science Foundation (2023), `https://nuclearsciencefuture.org/`.

[53] S. A. Giuliani, Z. Matheson, W. Nazarewicz, E. Olsen, P.-G. Reinhard, J. Sadhukhan, B. Schuetrumpf, N. Schunck, and P. Schwerdtfeger, "Colloquium: Superheavy elements: Oganesson and beyond," Rev. Mod. Phys. **91**, 011001 (2019), DOI: 10.1103/RevModPhys.91.011001.

[54] N. Schunck and D. Regnier, "Theory of nuclear fission," Prog. Part. Nucl. Phys. **125**, 103963 (2022), DOI: 10.1016/j.ppnp.2022.103963.

[55] I. Counts, J. Hur, D. P. L. Aude Craik, H. Jeon, C. Leung, J. C. Berengut, A. Geddes, A. Kawasaki, W. Jhe, and V. Vuletić, "Evidence for nonlinear isotope shift in Yb^+ search for new boson," Phys. Rev. Lett. **125**, 123002 (2020), DOI: 10.1103/PhysRevLett.125.123002.

[56] I. Angeli and K. P. Marinova, "Table of experimental nuclear ground state charge radii: An update," At. Data Nucl. Data Tables **99**, 69 (2013), DOI: 10.1016/j.adt.2011.12.006.

[57] S. Kraemer *et al.*, "Observation of the radiative decay of the ^{229}Th nuclear clock isomer," Nature **617**, 706 (2023), DOI: 10.1038/s41586-023-05894-z.